Supporting Information

High Fatigue Resistance of a Photochromic Dithienylethene Embedded into the Pores of a Metal-Organic Framework (MOF)

Heidi A. Schwartz,[a,b] Hannah Laurenzen,[a] Samuel Kerschbaumer,[b] Melanie Werker,[a] Selina Olthof,[c] Holger Kopacka[b], Hubert Huppertz,[b] Klaus Meerholz,[c] Uwe Ruschewitz*,[a]

[a] Institute of Inorganic Chemistry
University of Cologne
Greinstraße 6, D-50939 Cologne, Germany
E-mail: uwe.ruschewitz@uni-koeln.de

[b] Current affiliation: Institute of General, Inorganic, and Theoretical Chemistry
University of Innsbruck
Center for Chemistry and Biomedicine
Innrain 80-82, A-6020 Innsbruck, Austria

[c] Institute of Physical Chemistry
University of Cologne
Luxemburger Straße 116, D-50939 Cologne, Germany

Contents:

Description: size of DTE and pore sizes as well as BET surface areas of the used MOFs.

Fig. S1-S3 X-ray powder diffraction patterns of pristine MOF-5, MIL-68(In), and MIL-68(Ga).

Fig. S4 X-ray powder diffraction patterns of DTE@MOF-5 and unloaded, activated MOF-5.

Fig. S5 X-ray powder diffraction patterns of DTE@MIL-68(Ga) and unloaded, activated MIL-68(Ga).

Fig. S6 XPS data of DTE@MOF-5, DTE@MIL-68(In), and DTE@MIL-68(Ga).

Fig. S7-S8 DSC (blue) and TGA (red) curves of DTE@MIL-68(In) and DTE@MIL-68(Ga).

Fig. S9 TGA curves of pristine DTE, the activated MOF, and DTE@MOF.

Fig. S10 Reflection spectra of DTE@MOF-5 and DTE@MIL-68(In).

Fig. S11 Reflection spectra of a neat powder of DTE.

Fig. S12 Reflection spectra of DTE@MOF-5, DTE@MIL-68(In), and DTE@MIL-68(Ga) recorded for the evaluation of the switching cycles.

Fig. S13 Absorption spectra (298 K) of DTE dissolved in ethanol and in acetone recorded for the evaluation of the switching cycles; switching cycles of DTE dissolved in ethanol and in acetone.

Fig. S14-S16 ^{1}H NMR spectra of DTE before and after UV light irradiation in DMSO-d_6 and DCl.

Fig. S17-S28 ^{1}H NMR spectra of digested solutions of DTE@MOF-5, DTE@MIL-68(In) and DTE@MIL-68(Ga) before and after UV light irradiation and in DMSO-d_6 and DCl.

Description:

1,2-bis[2-methylbenzo[b]thiophen-3-yl]3,3,4,4,5,5-hexafluoro-1-cyclopentene (DTE): From the reported crystal structure of DTE[1] the size of the open-ring form was estimated to 13.8 Å x 8.7 Å x 10.4 Å by taking the respective *van-der-Waals* radii into account. The elongations in each direction were estimated within *Diamond 4.4*[2] using the grid option. For the closed-ring form a size of 15.3 Å x 7.2 Å x 10.4 Å was estimated using *MarvinSketch*[3].

MOF-5: The crystal structure of MOF-5 consists of two differently sized cavities with a diameter of 15.1 Å and 11.0 Å, respectively taking the respective van-der-Waals radii into account.[4] The aperture of these cavities was given with 8 Å.[4] The surface area according to *Langmuir* was reported as 2900 m^2/g[4] corresponding to a BET surface area of 2296 m^2/g.[5] In our own measurements we obtained a BET surface area of 1467 m^2/g.

MIL-68(In)/MIL-68(Ga): The hexagonal channels of MIL-68(Ga)/MIL-68(In) have an aperture of 16-17 Å and the trigonal channels an aperture of 6 Å.[6] The BET surface areas were reported as 1117(24) m^2/g for MIL-68(Ga) and 746(31) m^2/g for MIL-68(In).[6] In our own measurements we obtained slightly higher values: 1560 m^2/g for MIL-68(Ga) and 1629 m^2/g for MIL-68(In).

Conclusion:

From the results above the porosity of the used MOFs increases from the MIL-68 compounds to MOF-5 taking their BET surface areas as a measure. Furthermore, the trigonal channels of MIL-68 are obviously too small to accommodate DTE molecules. However, the cavities of MOF-5 and the hexagonal channels of MIL-68 are obviously large enough to accommodate DTE molecules. This interpretation is corroborated by the results given in the main body of the manuscript.

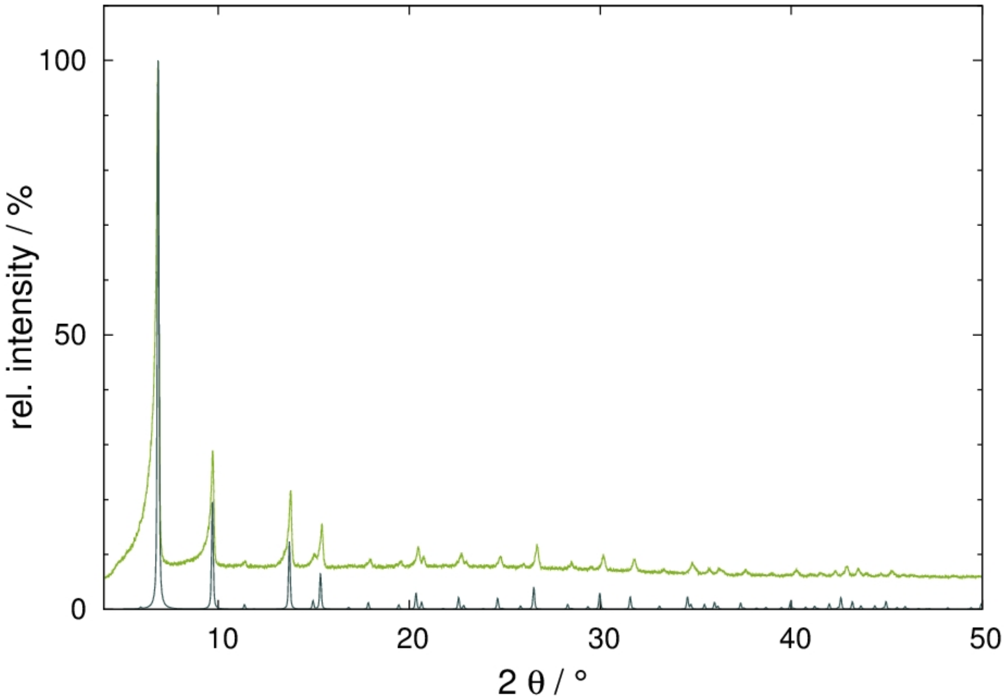

Fig. S1 XRPD pattern of activated MOF-5 (green curve; 298 K, *Huber G670*; λ = 1.54051 Å) compared to a pattern calculated from the known structure data of MOF-5 (blue curve).[4]

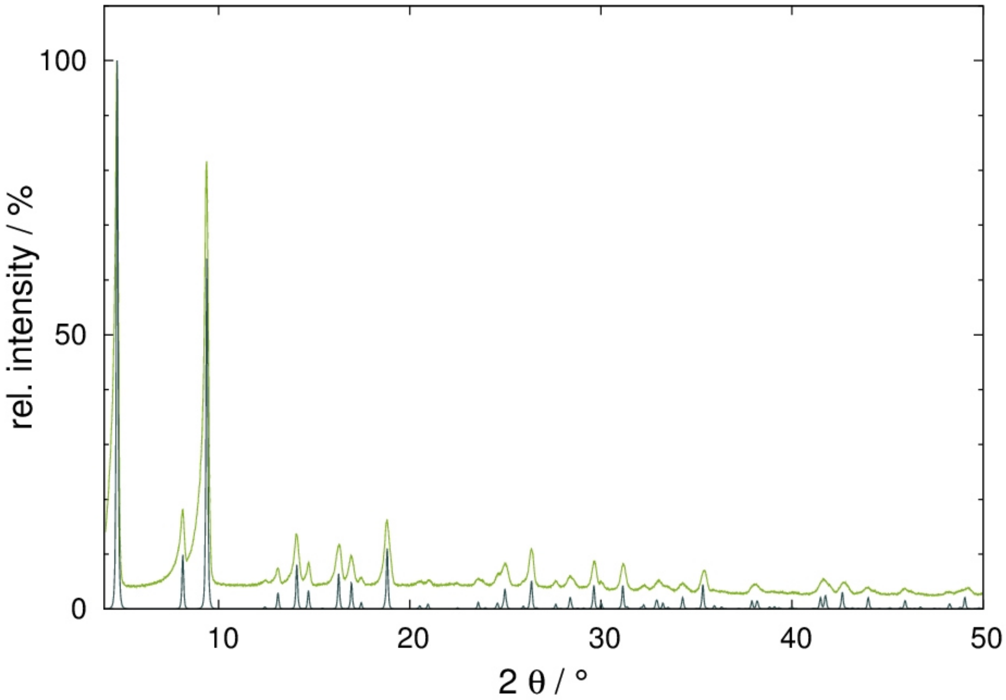

Fig. S2 XRPD pattern of activated MIL-68(In) (green curve; 298 K, *Huber G670*; λ = 1.54051 Å) compared to a pattern calculated from the known structure data of MIL-68(In) (blue curve).[6]

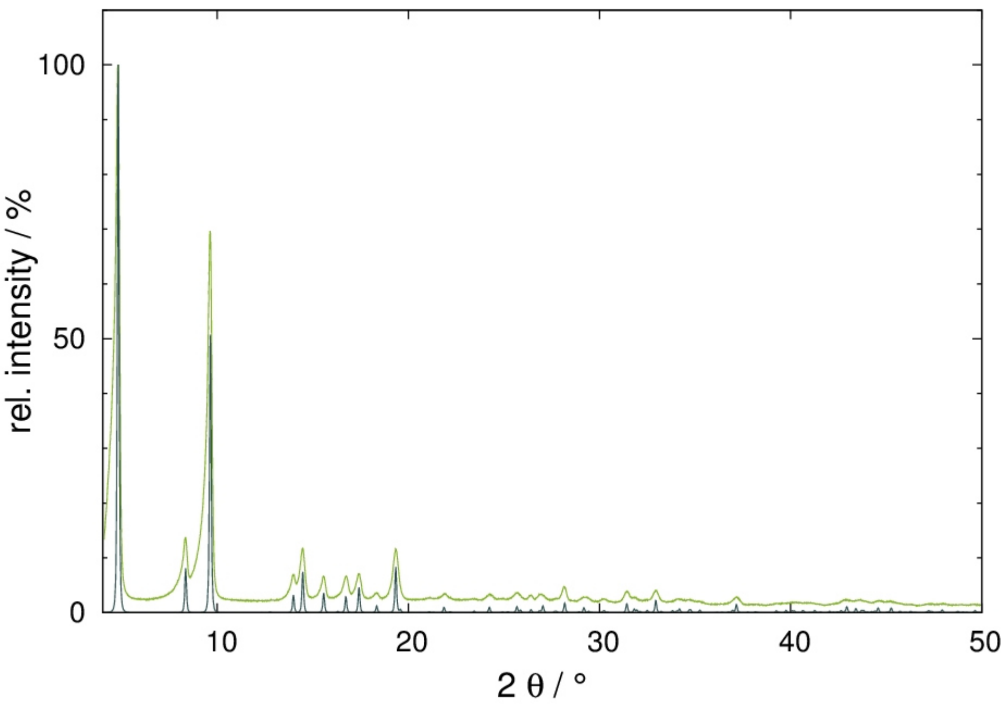

Fig. S3 XRPD pattern of activated MIL-68(Ga) (green curve; 298 K, *Huber G670*; λ = 1.54051 Å) compared to a pattern calculated from the known structure data of MIL-68(Ga) (blue curve).[6]

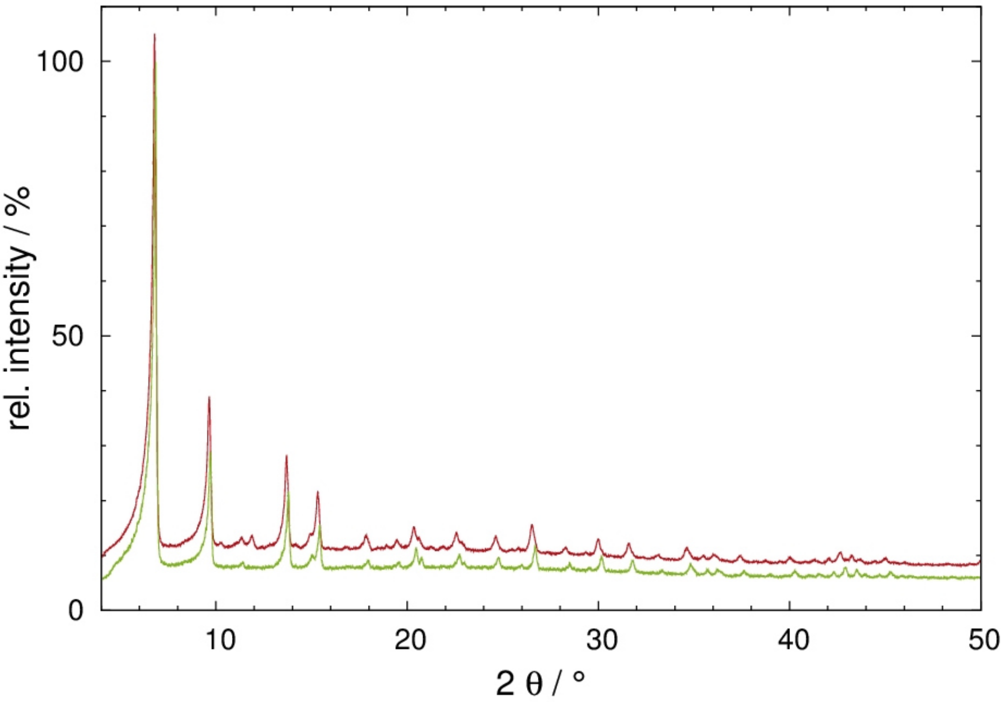

Fig. S4 XRPD patterns of DTE@MOF-5 (red curve) and unloaded, activated MOF-5 (green curve); 298 K, *Huber G670*; λ = 1.54051 Å; 5% offset along y axis.

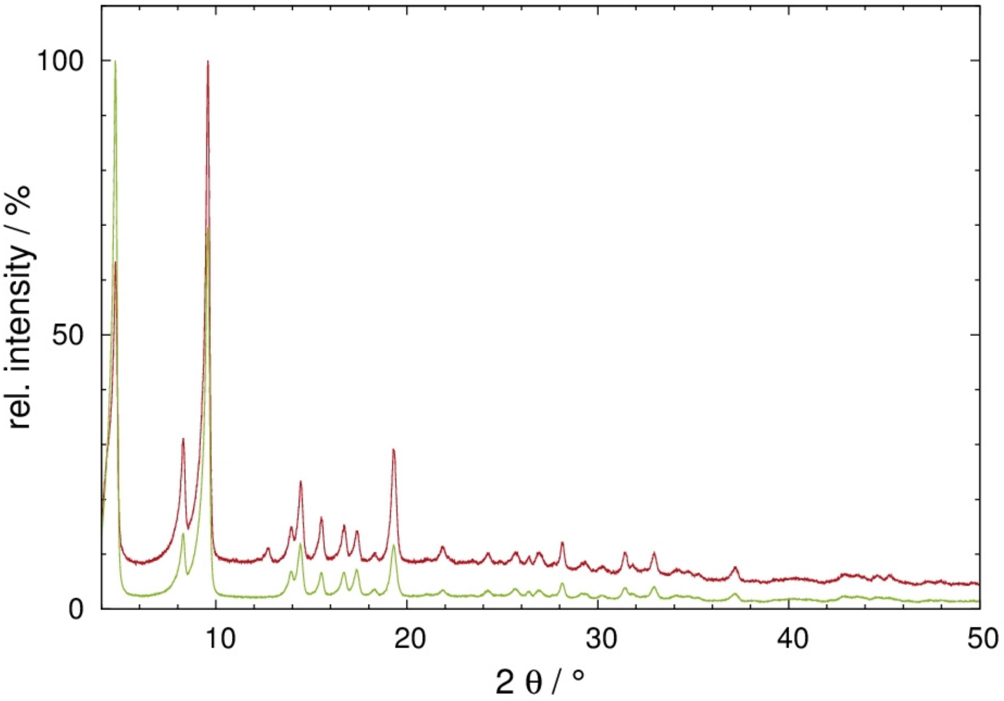

Fig. S5 XRPD patterns of DTE@MIL-68(Ga) (red curve) and unloaded, activated MIL-68(Ga) (green curve); 298 K, *Huber G670*; λ = 1.54051 Å; 5% offset along y axis.

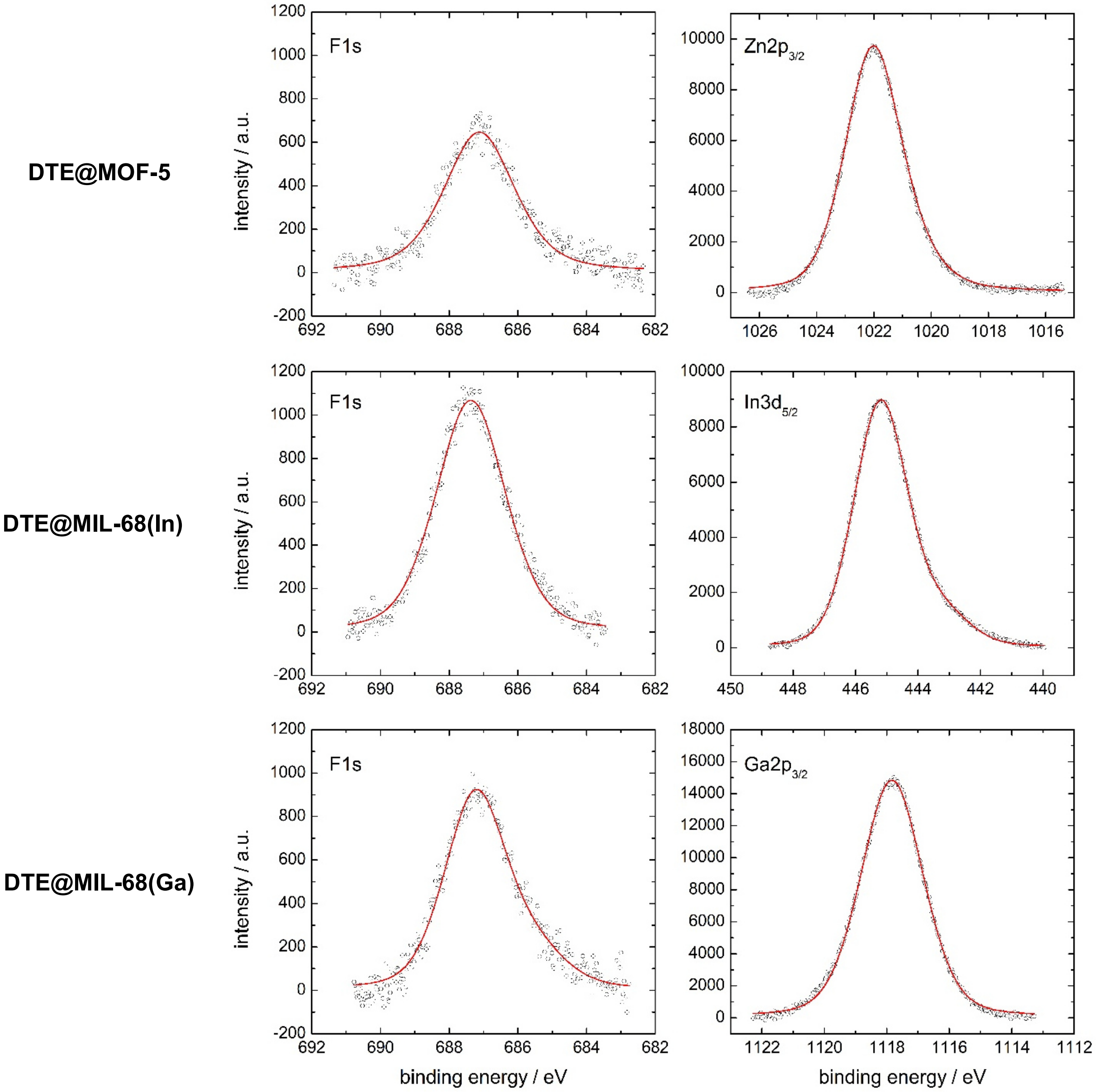

Fig. S6 XPS data of DTE@MOF-5, DTE@MIL-68(In), and DTE@MIL-68(Ga), both measurement data (grey) and peak fit (red) are shown.

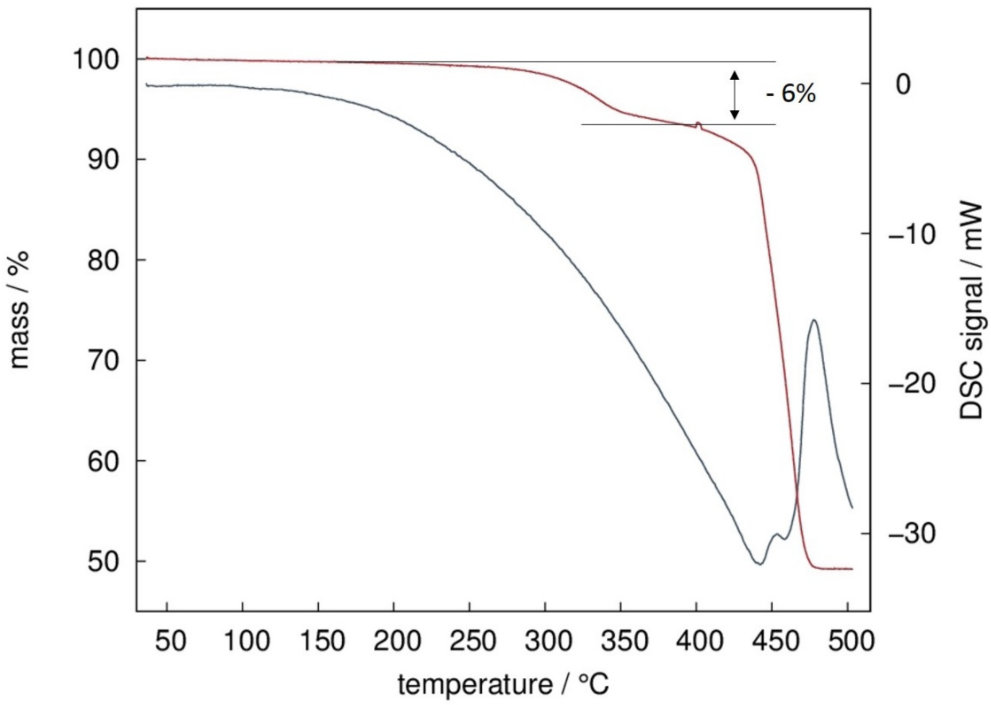

Fig. S7 DSC (blue) and TGA (red) curves of DTE@MIL-68(In).

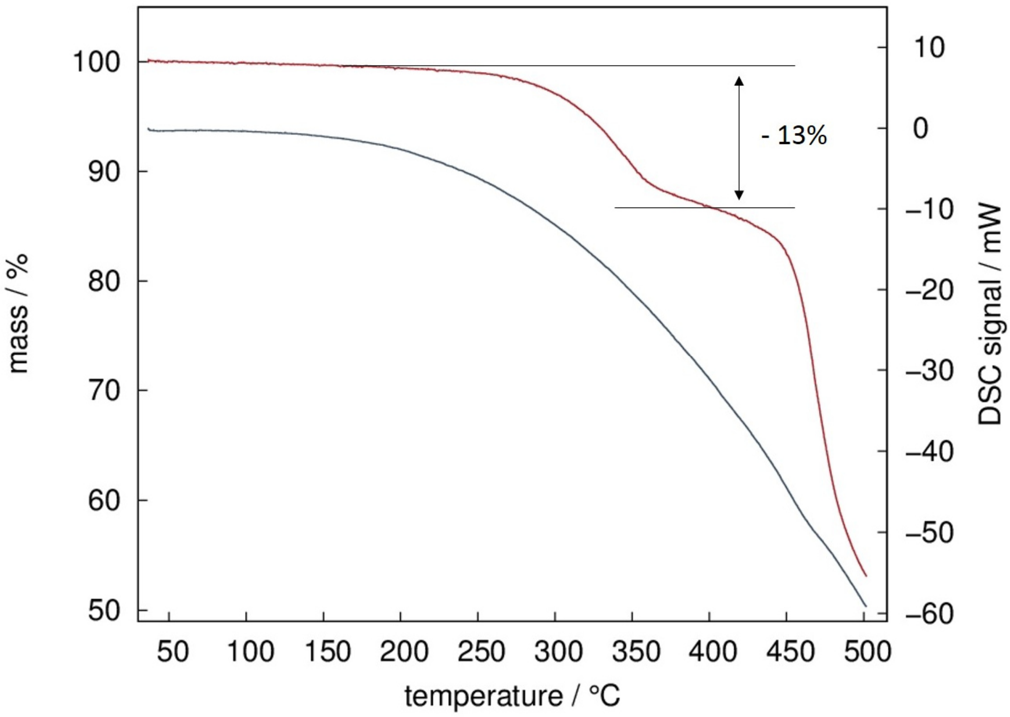

Fig. S8 DSC (blue) and TGA (red) curves of DTE@MIL-68(Ga).

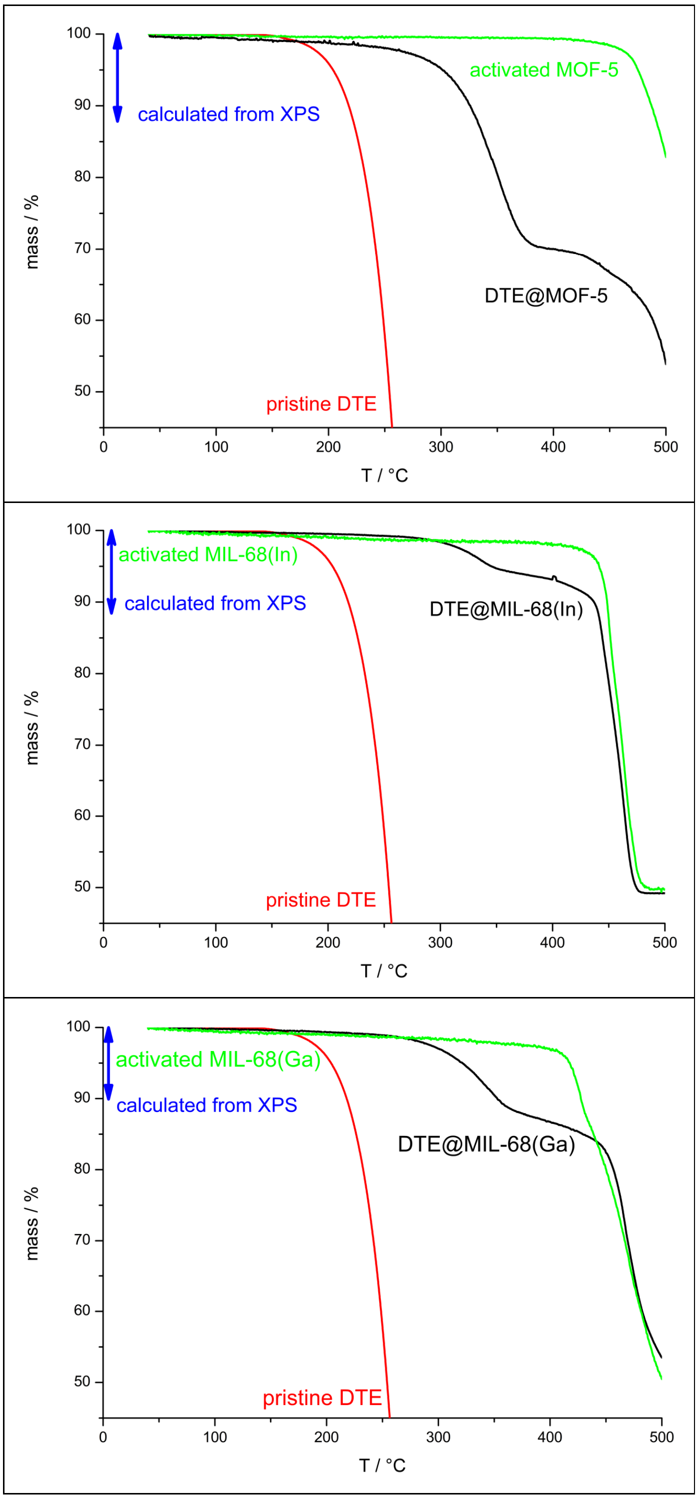

Fig. S9 TGA curves of pristine DTE (red curve), the activated MOF (green curve), and DTE@MOF (black curve). The expected mass loss for the release of DTE from DTE@MOF as obtained from the XPS data is marked with a blue arrow.

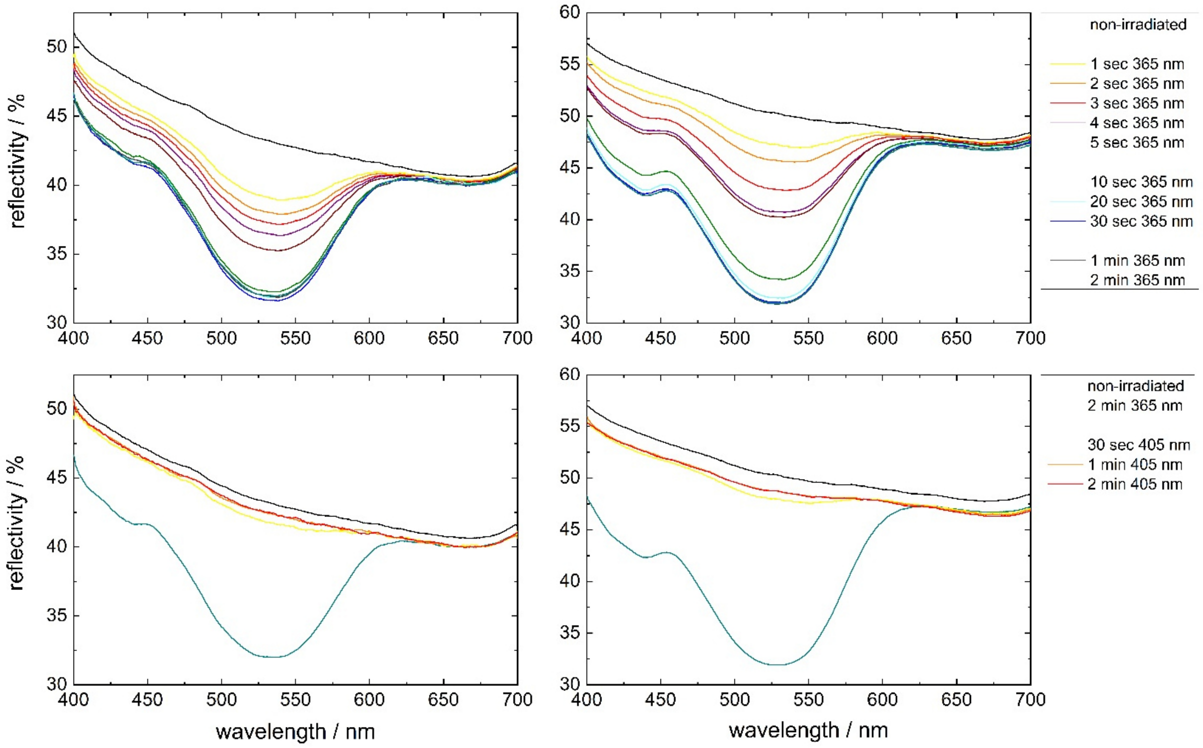

Fig. S10 Reflection spectra (298 K) of DTE@MOF-5 (left hand side) and DTE@MIL-68(In) (right hand side). First row: before and after stepwise irradiation with UV light (λ = 365 nm) and second row: before and after irradiation with UV light (*λ* = 365 nm, 2 min), followed by stepwise irradiation with visible light (*λ* = 405 nm).

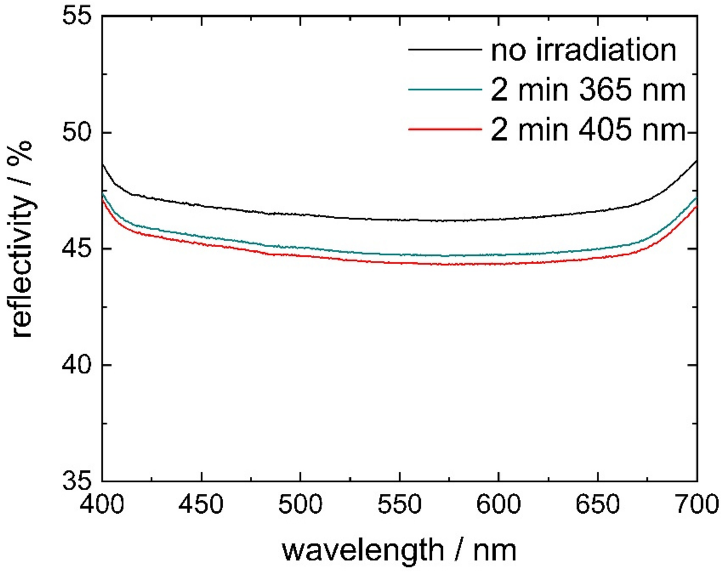

Fig. S11 Reflection spectra (298 K) of a neat powder of DTE before and after irradiation with UV light (*λ* = 365 nm, 2 min) and visible light (*λ* = 405 nm, 2 min), respectively.

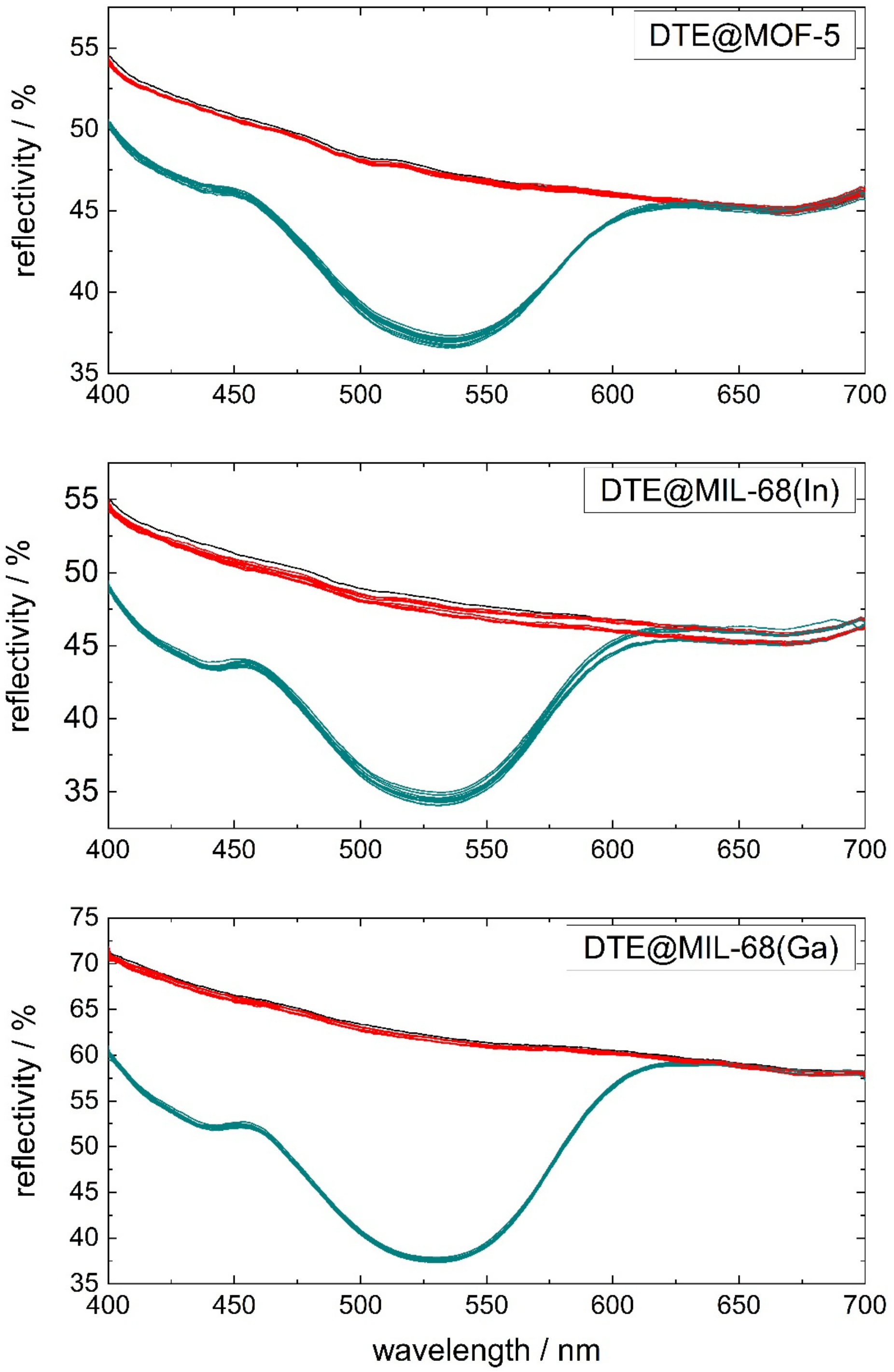

Fig. S12 Reflection spectra (298 K) of DTE@MOF-5 (top), DTE@MIL-68(In) (middle), and DTE@MIL-68(Ga) (bottom) recorded for the evaluation of the switching cycles (non-irradiated: black; λ = 365 nm, 2 min: cyan; λ = 405 nm, 2 min: red).

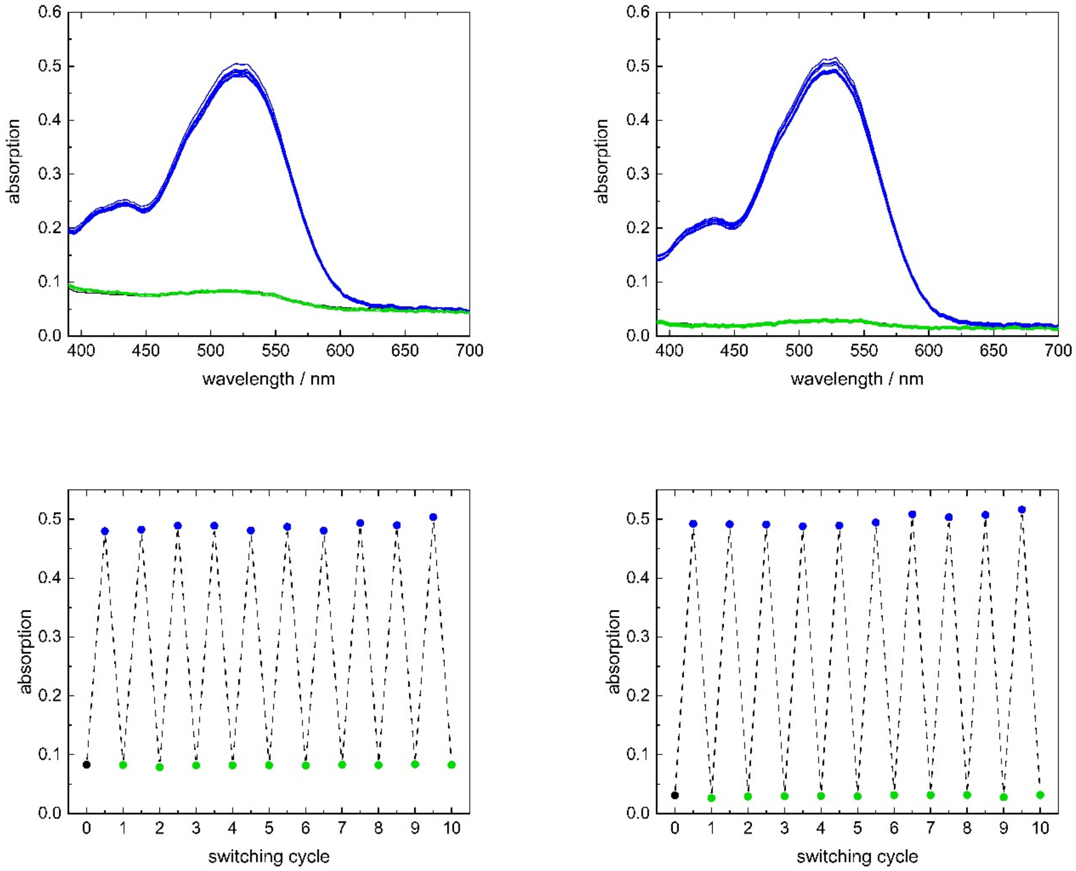

Fig. S13 Top: Absorption spectra (298 K) of DTE dissolved in ethanol (top, left) and in acetone (top, right) recorded for the evaluation of the switching cycles (non-irradiated: black; λ = 365 nm, 2 min: cyan; λ = 535 nm, 2 min: red); bottom: switching cycles of DTE dissolved in ethanol (bottom, left) and in acetone (bottom, right).

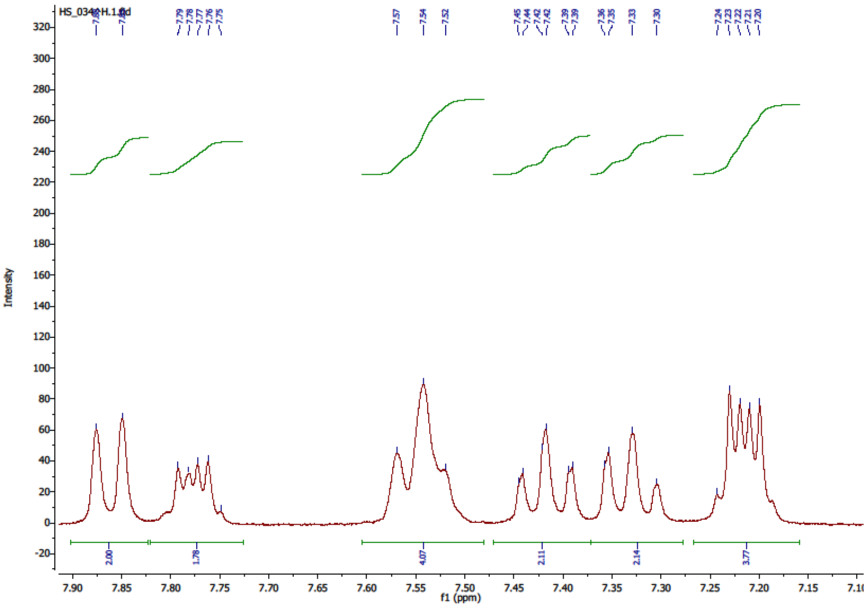

Fig. S14 ^{1}H NMR spectrum of DTE emphasizing the aromatic region. The spectrum was recorded in DMSO-d_6 after addition of DCl.

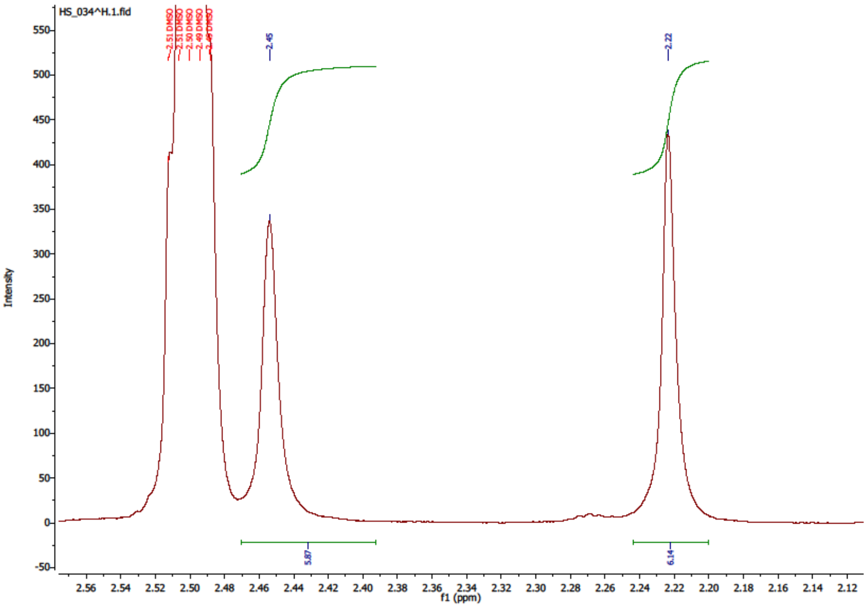

Fig. S15 ^{1}H NMR spectrum of DTE emphasizing the methyl region. The spectrum was recorded in DMSO-d_6 after addition of DCl.

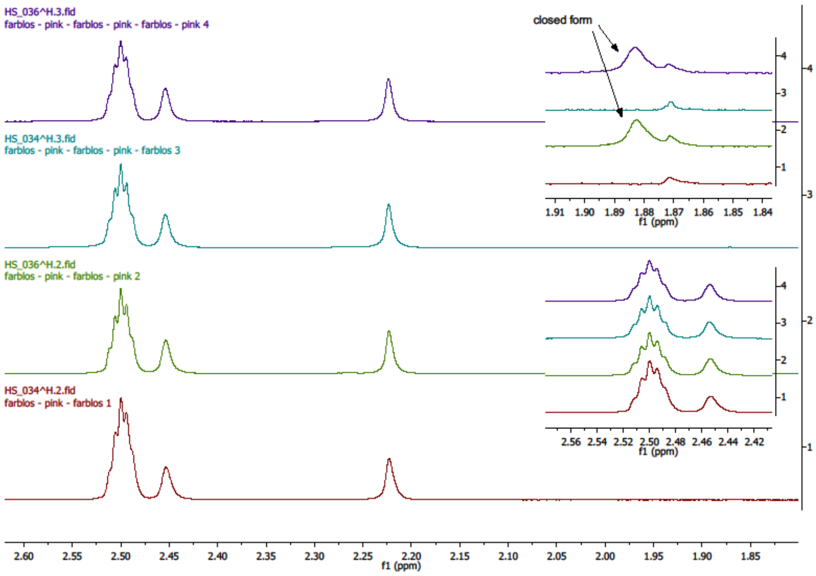

Fig. S16 ^{1}H NMR spectra of DTE after two switching cycles (red line: colourless state, green line: after UV light irradiation, blue line: after visible light exposure, purple line: after UV light irradiation). The spectra were recorded in DMSO-d_6 after addition of DCl.

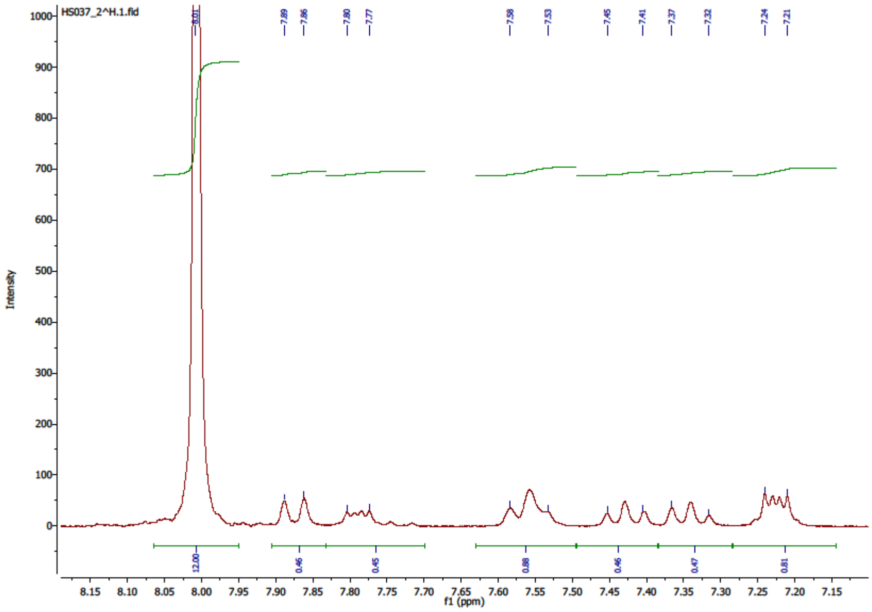

Fig. S17 ^{1}H NMR spectrum of non-irradiated DTE@MOF-5 focusing on the aromatic region. The spectrum was recorded in DMSO-d_6 after addition DCl.

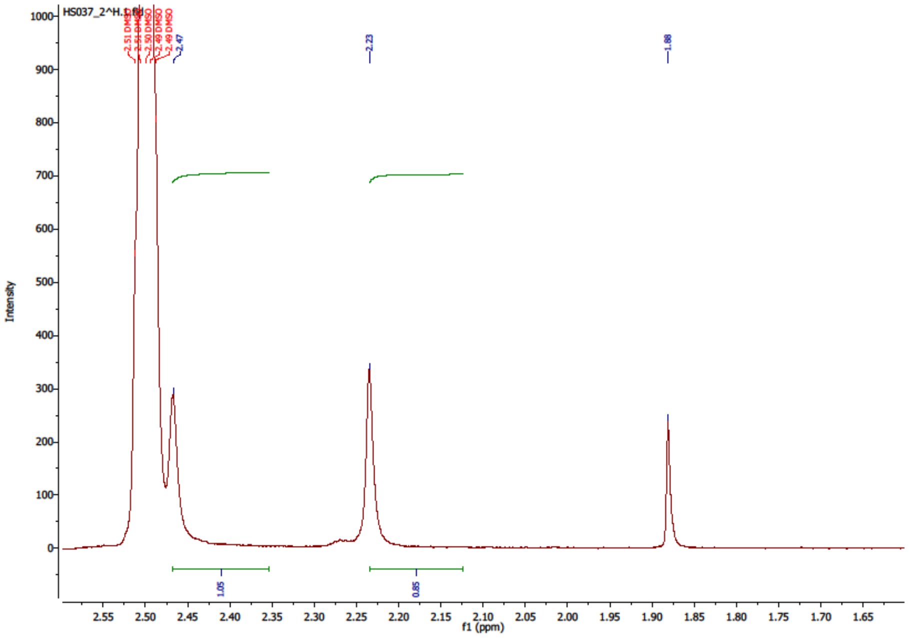

Fig. S18 ^{1}H NMR spectrum of non-irradiated DTE@MOF-5 focusing on the methyl region. The spectrum was recorded in DMSO-d_6 after addition DCl. The signal at 1.88 ppm is attributed to side products after addition of DCl.

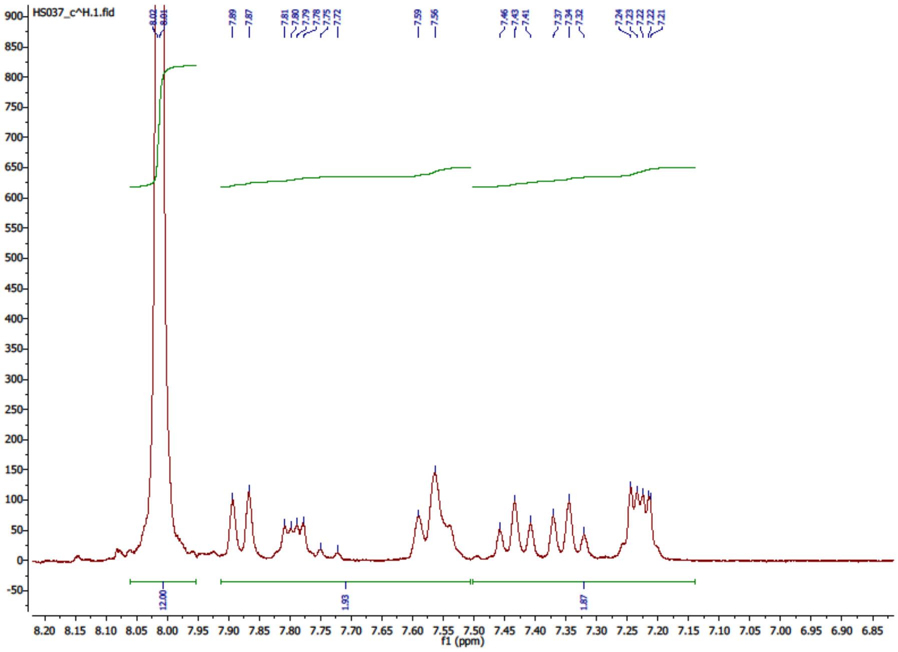

Fig. S19 ^{1}H NMR spectrum of DTE@MOF-5 after 15 min of UV light irradiation (λ = 365 nm) focusing on the aromatic region. The spectrum was recorded in DMSO-d_6 after addition DCl.

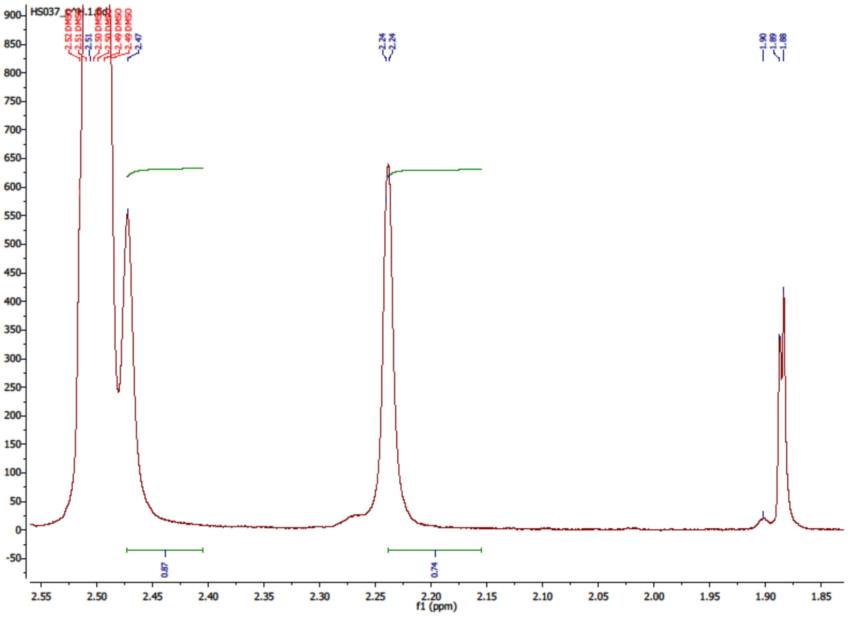

Fig. S20 ^{1}H NMR spectrum of DTE@MOF-5 after 15 min of UV light irradiation (λ = 365 nm) focusing on the methyl region. The spectrum was recorded in DMSO-d_6 after addition DCl.

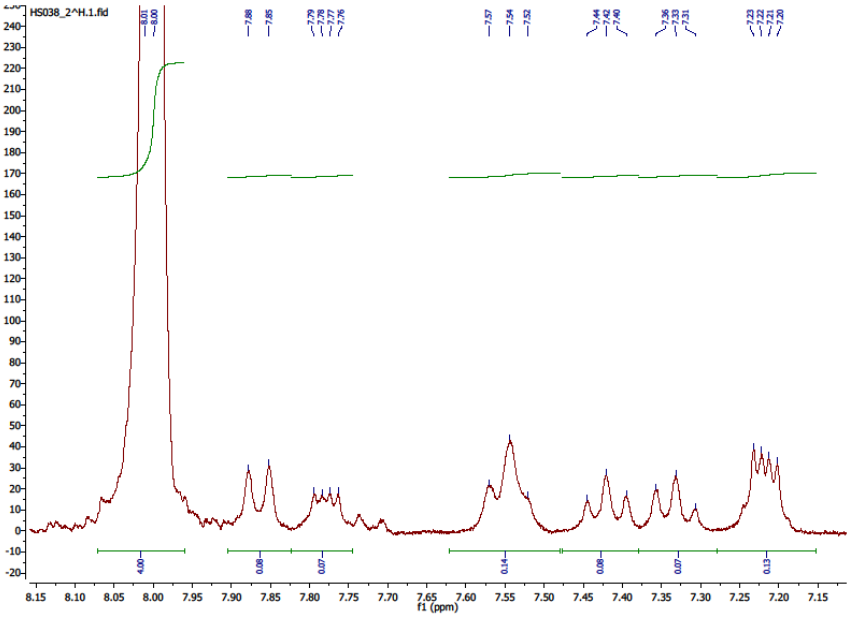

Fig. S21 ^{1}H NMR spectrum of non-irradiated DTE@MIL-68(In) focusing on the aromatic region. The spectrum was recorded in DMSO-d_6 after addition DCl.

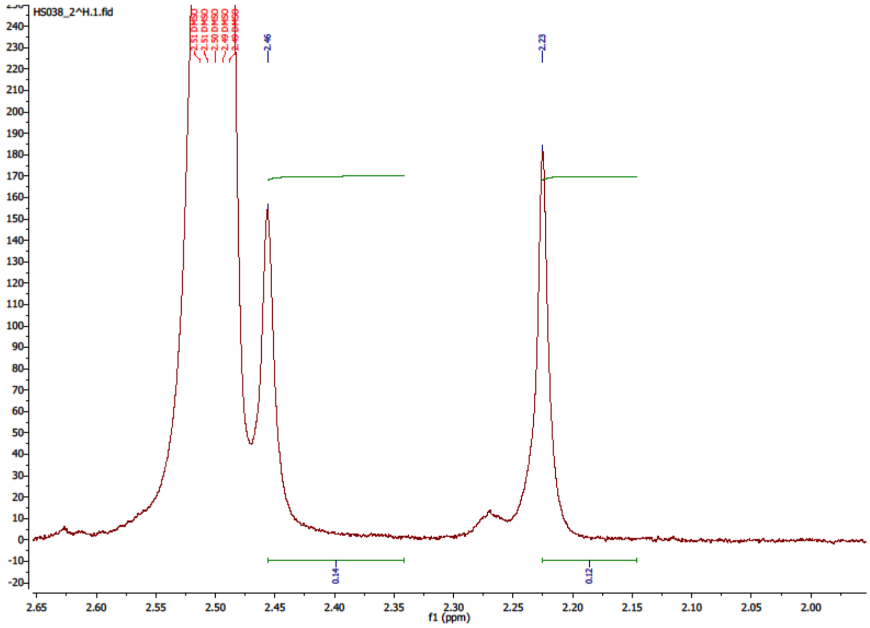

Fig. S22 ^{1}H NMR spectrum of non-irradiated DTE@MIL-68(In) focusing on the methyl region. The spectrum was recorded in DMSO-d_6 after addition DCl.

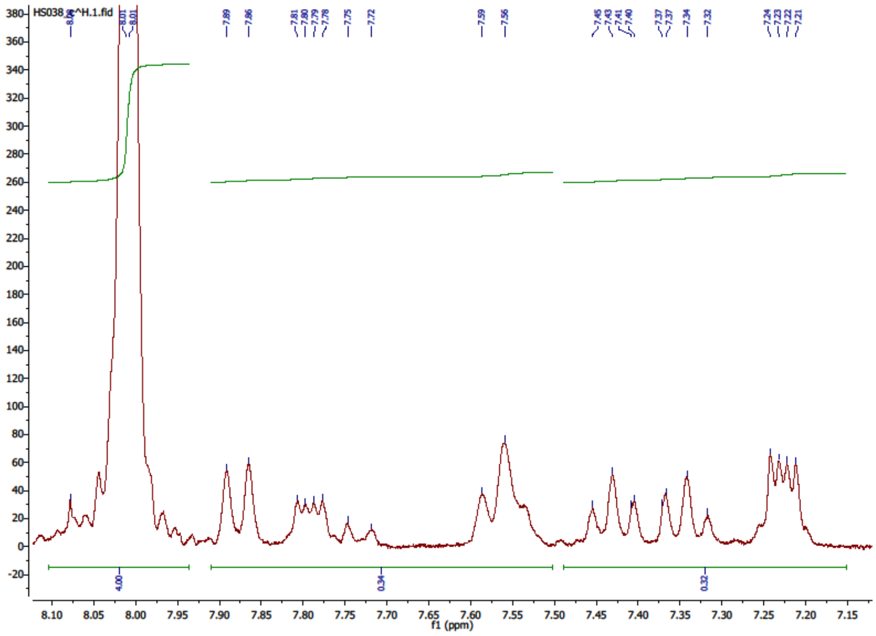

Fig. S23 ^{1}H NMR spectrum of DTE@MIL-68(In) after 15 min of UV light irradiation (λ = 365 nm) focusing on the aromatic region. The spectrum was recorded in DMSO-d_6 after addition DCl.

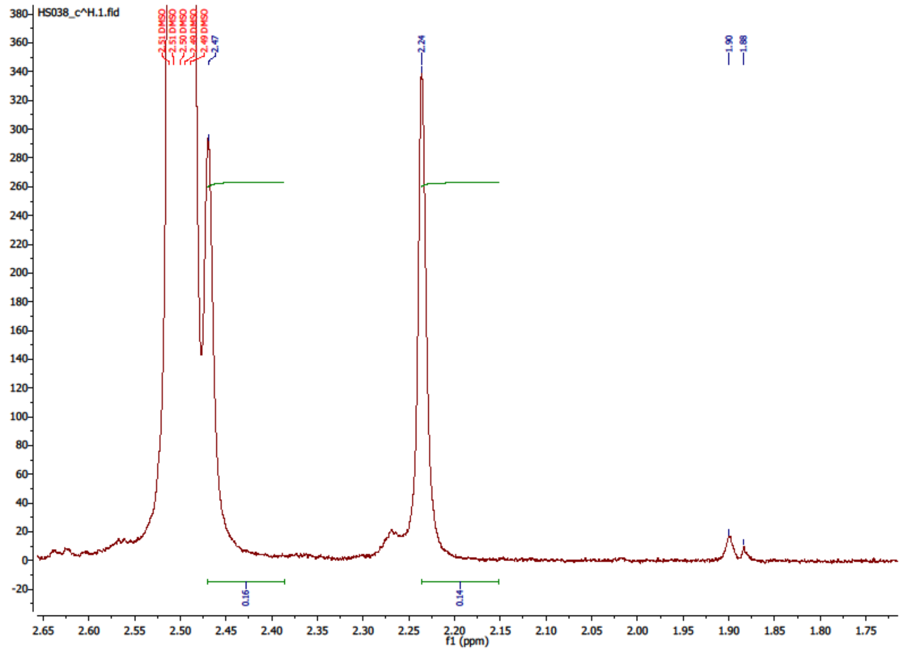

Fig. S24 ^{1}H NMR spectrum of DTE@MIL-68(In) after 15 min of UV light irradiation (λ = 365 nm) focusing on the methyl region. The spectrum was recorded in DMSO-d_6 after addition DCl.

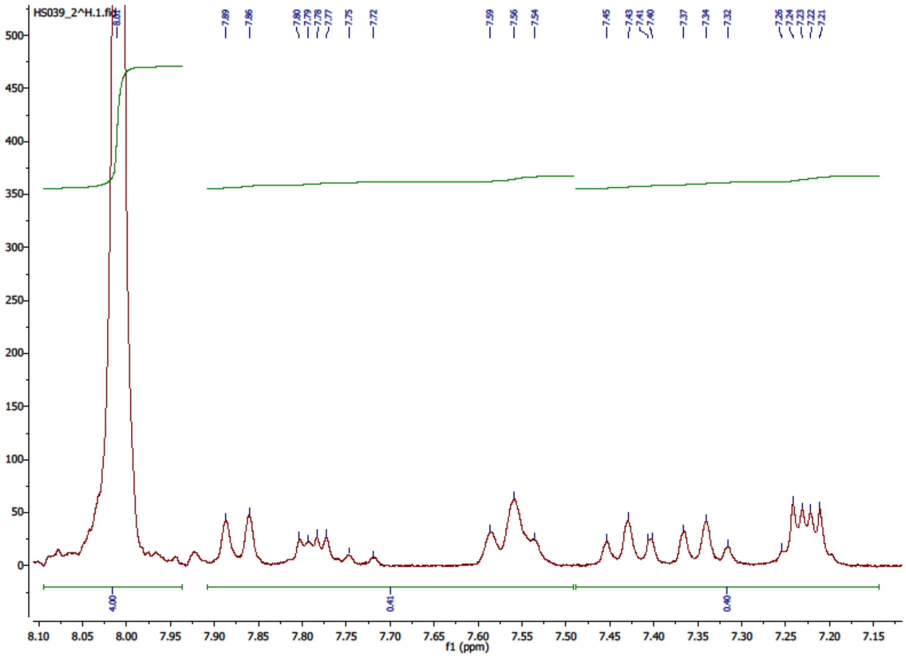

Fig. S25 ^{1}H NMR spectrum of non-irradiated DTE@MIL-68(Ga) focusing on the aromatic region. The spectrum was recorded in DMSO-d_6 after addition DCl.

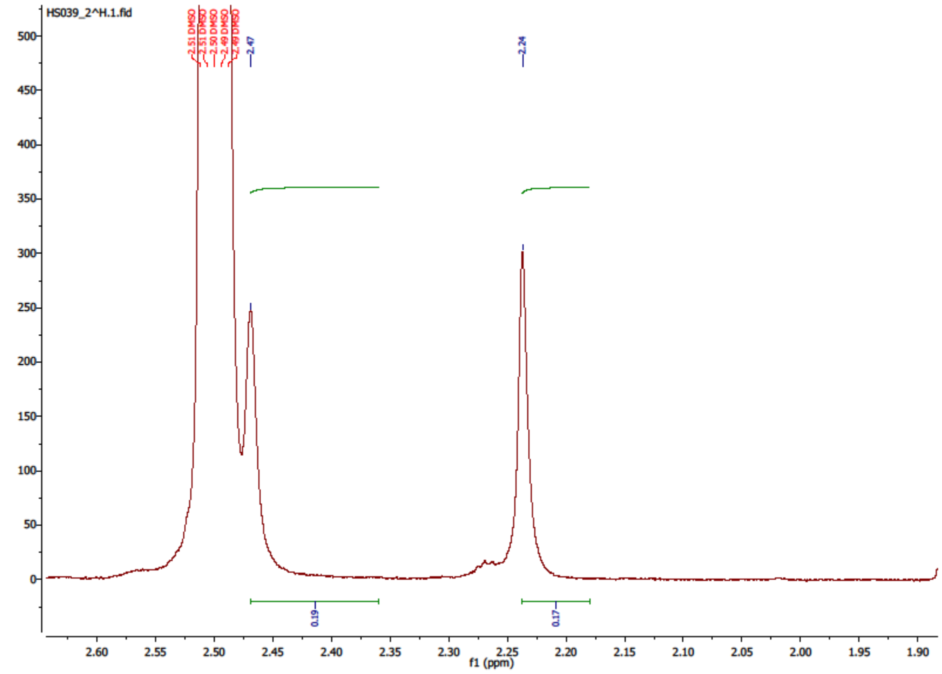

Fig. S26 ^{1}H NMR spectrum of non-irradiated DTE@MIL-68(Ga) focusing on the methyl region. The spectrum was recorded in DMSO-d_6 after addition DCl.

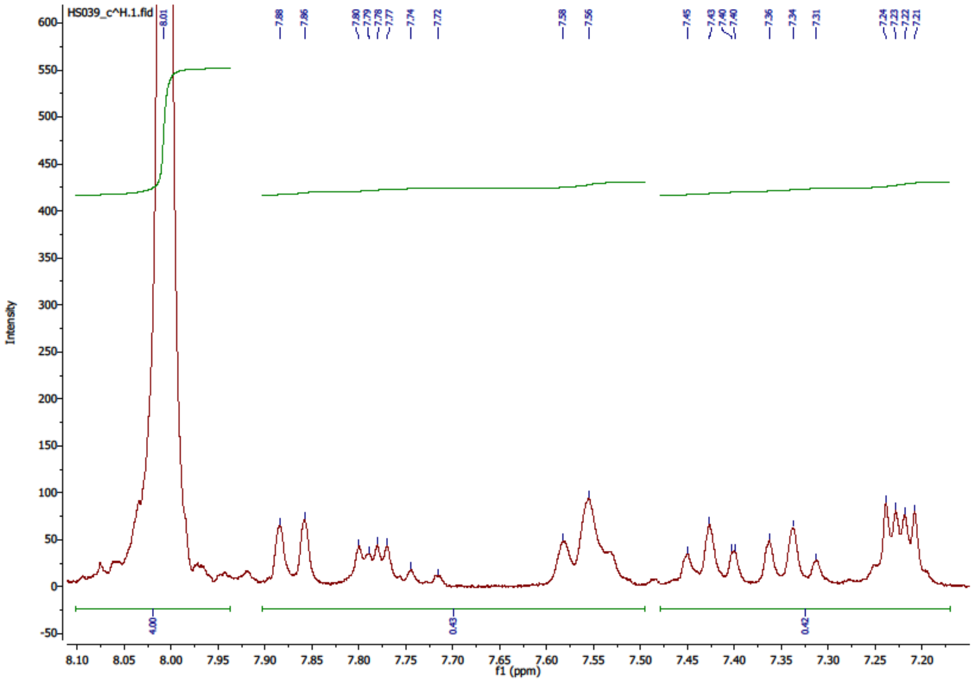

Fig. S27 ^{1}H NMR spectrum of DTE@MIL-68(Ga) after 15 min of UV light irradiation (λ = 365 nm) focusing on the aromatic region. The spectrum was recorded in DMSO-d_6 after addition DCl.

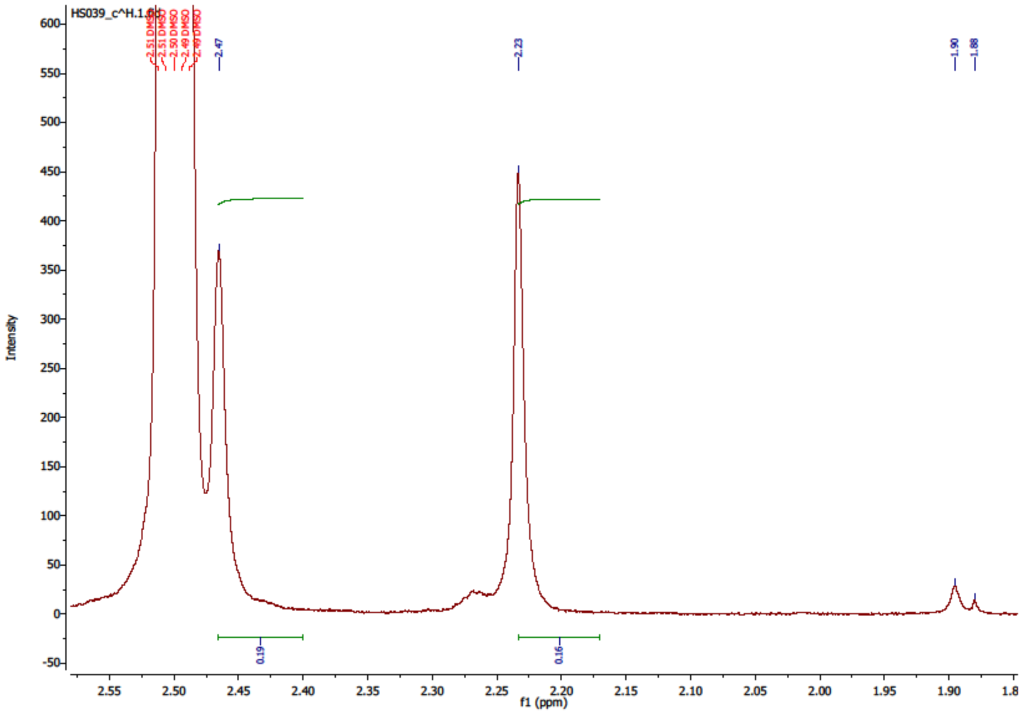

Fig. S28 ^{1}H NMR spectrum of DTE@MIL-68(Ga) after 15 min of UV light irradiation (λ = 365 nm) focusing on the methyl region. The spectrum was recorded in DMSO-d_6 after addition DCl.

References

[1] T. Yamaguchi, K. Uchida, M. Irie, *Bull. Chem. Soc. Jpn.* **2008**, *81*, 644–652.

[2] K. Brandenburg, *Diamond 4.4*, Crystal Impact GbR, Bonn, **2017**.

[3] *MarvinSketch*, Version 19.6, **2019**, ChemAxon (http://www.chemaxon.com).

[4] H. Li, M. Eddaoudi, M. O'Keeffe, O. M. Yaghi, *Nature* **1999**, *402*, 276–279.

[5] G. Férey, *Chem. Soc. Rev.* **2008**, *37*, 191–214.

[6] C. Volkringer, M. Meddouri, T. Loiseau, N. Guillou, J. Marrot, G. Férey, M. Haouas, F. Taulelle, N. Audebrand, M. Latroche, *Inorg. Chem.* **2008**, *47*, 11892–11901.